Dispersion relation analysis of $d + {}^{208}Pb$ elastic scattering

Y. Wang,* C. C. Foster, E. J. Stephenson, and Li Yuan
Indiana University Cyclotron Facility, Bloomington, Indiana 47408

J. Rapaport
Ohio University, Athens, Ohio 45701
(Received 20 December 1991)

Elastic scattering of deuterons from ^{208}Pb in the energy range $E_d = 9$ to 79.2 MeV is analyzed using a dispersive optical model potential (OMP). In this analysis, a dispersion relation connects the volume integrals of the imaginary and the real parts of the OMP. Best-fit dispersive OMP parameters are obtained from fits to experimental cross-section and analyzing power data at one energy, and dispersive OMP parameters with a smooth energy dependence are determined from fits to the entire data set. Comparisons, showing fits of similar quality, of the predictions of the cross sections and analyzing powers given by the best-fit dispersive OMP and standard OMP are presented. Dispersive OMP parameters with a smooth energy dependence also give a good description of the experimental data.

PACS number(s): 24.10.Ht, 24.70.+s, 25.45.De

I. INTRODUCTION

In recent years, a great deal of theoretical attention has been devoted to the development of an optical model potential (OMP) that represents a consistent formulation of the nucleon-nucleus mean field at both positive and negative energies [1–6]. In this unified description the real central OMP is defined with two terms. One, which varies slowly with energy, is taken to represent the local equivalent of the energy-independent but nonlocal "Hartree-Fock" component of the nuclear mean field. The second or "correction" term, which often manifests a more complicated radial and energy dependence, is derived at positive energies from a phenomenological complex potential based on a dispersion relation (a consequence of causality). The combined potential, also called a dispersive OMP, may be extrapolated to negative energies where it is taken to represent the mean field of the bound nucleons.

The dispersive optical model has been successfully applied to an understanding of the energy dependence of the optical potential for the $n + {}^{208}Pb$ and $p + {}^{208}Pb$ systems [5,6]. The extrapolated potential also successfully describes bound-state properties such as single-particle energies, occupation probabilities, and absolute spectroscopic factors. This success suggests that it may be profitable to apply this model to composite particle scattering, at least at positive energies. These attempts have been successful in the study of the energy dependence of the real central potential for $^{208}Pb(^{16}O,^{16}O)^{208}Pb$ and $^{40}Ca(\alpha,\alpha)^{40}Ca$ elastic scattering as reported by Mahaux *et al.* [1]. In those studies, the composite particle analogues to the bound-state problem at negative energies were not investigated.

In this paper, the dispersive optical model is applied for the first time to the analysis of $d + {}^{208}Pb$ elastic scattering. The dispersion relation used previously for the nucleus-nucleus case [1] is employed in the present study. This dispersion relation is distinguished from the nucleon-nucleus version by the absence of the correlation component in the correction term [1,2] for the real central potential.

The study of composite projectiles also requires a prescription for the selection for the Fermi energy, the lower limit of the dispersion relation integral. Ioannides and Johnson [7] studied deuteron propagation through nuclear matter and finite-size nuclei, and found that the "deuteron" is less bound in the nucleus than in free space, especially at low bombarding energies, and that it may be regarded as an n-p pair. Thus we have chosen the deuteron Fermi energy to be the sum of the neutron and proton values [1,8], i.e., $E_F = -11.56$ MeV for ^{208}Pb. The real part of the dispersive OMP, evaluated in the positive-energy region by fitting the $d + {}^{208}Pb$ elastic-scattering data, may be extrapolated into the negative-energy region. This extrapolated potential might be useful in the study of the bound-state properties for n-p pairs even though there are no bound deuteron states in the same sense as there are bound single-particle states in the nucleus.

In a nucleon-nucleus dispersive analysis, a set of optical-model parameters are obtained that provide a good fit to a large set of scattering data (positive energies) as well as bound-state information (negative energies). In these analyses [1–5], it is usual to assume that the geometrical parameters of the imaginary part of the OMP are independent of energy. This simplifies the integrals in the dispersion analysis and results in analytic forms for the correction terms. Similarly, analytic forms for the energy

*Present address: Physics Department, Kent State University, Kent, OH 44242.

dependence of potential depths are also assumed. In the present analysis, we take a somewhat different approach. The constraints of the dispersive analysis are applied to the volume integrals of the potential, since they are better determined by the data than any single geometric parameter. Initial values of the volume integrals are obtained from best fits applying a standard OMP to individual data sets. These volume integrals exhibit a smooth and easily parametrized energy dependence. In the subsequent search using dispersive constraints, the volume integrals of the imaginary terms are kept fixed at the parametrized values. The volume integrals of the correction terms in the real central potential are evaluated using the volume integrals of the imaginary potentials through the dispersions relation (see Sec. III). In this way, the energy dependence of the volume integrals of the imaginary potentials and the correction terms are determined before the search for individual dispersive OMP parameters. The resulting dispersive OMP typically has a smooth energy dependence. This is helpful for interpolating the OMP parameters to other energies.

The database used in the dispersion analysis is discussed in Sec. II. The formulation of the dispersive OMP is described in detail in Sec. III. The results of the dispersive OMP individual best-fit analyses are presented in Sec. IV, while we present in Sec. V the dispersive OMP with smooth energy dependence for deuteron scattering from ^{208}Pb. Section VI is devoted to discussion and Sec. VII presents a summary of this study.

II. THE DATABASE USED IN THE DISPERSIVE ANALYSIS

We have made use of deuteron scattering data [9–16] from ^{208}Pb that have been published in the energy interval between 8 and 90 MeV. At some energies the data consist of just differential cross-section measurements, while at other energies, both cross section and analyzing power measurements have been reported. While the differential cross section and vector analyzing power are sensitive primarily to the central and spin-orbit components of the OMP, the tensor analyzing powers are sensitive in addition to spin-1 tensor terms. Since the focus of this study is on the relationship between the real and imaginary parts of the central potential, we have chosen to exclude tensor analyzing power data from the analysis. A real spin-orbit potential is included as an essential part of the description of the vector analyzing power data. One possible extension of this work would be to introduce an imaginary spin-orbit term, possibly at the higher bombarding energies, and to expand the dispersive model to include this spin dependence.

All of the elastic-scattering data sets have been reproduced using the standard optical model [9–16]. We classify these OMP parameters into four sets, based on the method used in the analysis. The OMP parameters in sets I and II are those tabulated in Ref. [9]. Set I with data in the energy range $8 \leq E_d \leq 90$ MeV has no spin-orbit term and reproduces only elastic differential cross section measurements. Set II contains the same data as set I (only differential cross sections), but includes a spin-orbit potential in the optical model analysis. In set III, the OMP parameters were obtained by Murayama *et al.* [10] using a potential with central and spin-orbit terms fit to data sets containing both cross section and analyzing power information in the energy range $10 \leq E_d \leq 23$ MeV. However, in this analysis, the potential was constrained to allow only the variation of the real and imaginary central potential depths. The rest of the parameters in the potential were held constant at values similar to those given in Ref. [17]. The set IV parameters [11–16] were obtained by fitting central and spin-orbit terms without constraints to data sets containing both cross section and analyzing power information in the energy range $9 \leq E_d \leq 79.2$ MeV.

In order to complete the dispersive analysis of the $d + ^{208}$Pb data in the way described in Sec. I, a smooth energy-dependent set of volume integrals must be obtained from the standard OMP parameters. The volume integral per nucleon of the real and imaginary central potentials, J_V and J_W, are shown in Fig. 1. Both volume-integral sets that are based solely on cross section data (potential sets I and II) show considerable variation.

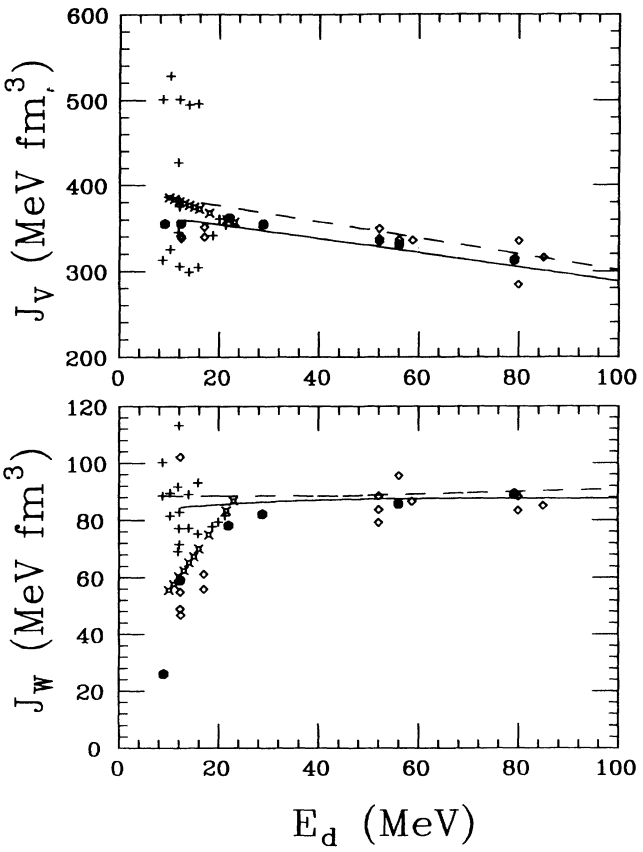

FIG. 1. Energy dependence of the volume integrals of the real and imaginary central optical potentials for deuteron elastic scattering. The cross, diamond, fancy square, and filled circles refer to optical potential sets I, II, III, and IV, respectively. The solid lines denote the global optical potential of Daehnick *et al.* [17] and the dashed lines refer to the global optical potential of Bojowald *et al.* [19].

Thus, they would not make a satisfactory basis on which to understand the energy dependence. The parameters of potential set III have a smooth energy dependence that is an artifact of the constraint of the potential geometry. In contrast, the values from potential set IV appear to vary smoothly with energy in a manner similar to the nucleon dependence of Ref. [5]. Thus we have restricted our consideration to only this set. These data, available at energies of $E_d=9.0$, 12.3, 22.0, 28.8, 56.0, and 79.2 MeV, provide good coverage of the energy regime below 100 MeV. Once the analysis was underway, we obtained new data, which contained both cross sections and vector analyzing powers at $E_d=15.0$, and 18.0 MeV from Ref. [10] and $E_d=20.0$ and 52.0 MeV from Ref. [18]. The data are compared with the predictions given by the present dispersive OMP in Sec. V.

The solid and dashed lines in Fig. 1 indicate the calculated energy dependence of the global optical potentials of Daehnick [17] and Bojowald [19], respectively. Both global optical potentials give good descriptions for the volume integrals of the imaginary part of the optical potentials, the sets I–IV, above about 30 MeV, but fail for the sets II–IV at lower energies. The predicted volume integral for the real central potential follows the average trend of the empirical data.

III. DISPERSION OMP FORMALISM

The deuteron-nucleus OMP, $U(r,E)$, is given by

$$U(r,E)=V_C(r)-U_D(r,E)-U_{\text{s.o.}}(r,E) , \tag{1}$$

where the $V_C(r)$ is the Coulomb potential and is taken to be that of a charged sphere of radius $R_C=r_C A^{1/3}$. $U_D(r,E)$ is the central part of the deuteron-nucleus optical potential and $U_{\text{s.o.}}(r,E)$ is the spin-orbit part. The central part is defined as [17]

$$\begin{aligned} U_D(r,E)&=V(r,E)+iW(r,E)\\ &=V_V(E)f(r,R_V,a_V)+iW_S(E)f(r,R_W,a_W)\\ &\quad -i4a_D W_D(E)\frac{d}{dr}f(r,R_W,a_W) , \end{aligned} \tag{2}$$

where $f(r,R_j,a_j)$ with $j=V,W$ is the Woods-Saxon form. $W(r,E)$ is the sum of the volume part $W_S(r,E)$ and the surface part $W_D(r,E)$. While the geometrical parameters may vary with energy, here we emphasize the independence of the potential depths and the geometry.

In the dispersion relation treatment [1], the real term $V(r,E)$ consists of a term slowly varying with energy, $V_0(r,E)$, plus a correction term $\Delta V(r,E)$, which is calculated using a dispersion relation, so that

$$U_D(R,E)=V_0(r,E)+\Delta V(r,E)+iW(r,E) . \tag{3}$$

In the nucleon-nucleus case, the $V_0(r,E)$ term is called the Hartree-Fock term $V_{\text{HF}}(r,E)$. The correction term $\Delta V(r,E)$ can be evaluated from the subtracted dispersion relation in nucleus-nucleus scattering [1], which may be expressed in the deuteron-nucleus case as

$$\Delta V(r,E)=(E_F-E)\frac{\text{P}}{\pi}\int_{E_F}^{\infty}\frac{W(r,E')}{(E'-E_F)(E-E')}dE' . \tag{4}$$

The symbol P denotes the principal value. In the deuteron-nucleus system, the correlation component of $\Delta V(r,E)$ is absent [1]. E_F is the sum of the proton and neutron Fermi energies [1,8].

We will make the connection between the imaginary potential and the real correction term though the volume integral per nucleon,

$$J_W(E)=\frac{4\pi}{A_T A_d}\int W(r,E)r^2dr , \tag{5}$$

where A_T and A_d are the masses of the target and projectile deuteron, respectively. The subtracted dispersion relation [see Eq. (4)] stated in terms of the volume integral is

$$J_{\Delta V}(E)=(E_F-E)\frac{\text{P}}{\pi}\int_{E_F}^{\infty}\frac{J_W(E')}{(E'-E_F)(E-E')}dE' . \tag{6}$$

The absorptive term $W(r,E)$ consists of a volume part $W_S(r,E)$ and a surface part $W_D(r,E)$. Thus the volume integral $J_{\Delta V}(E)$ can be expressed as the sum of a volume and surface part, $J_{\Delta V_S}(E)$ and $J_{\Delta V_D}(E)$:

$$J_{\Delta V_S}(E)=(E_F-E)\frac{\text{P}}{\pi}\int_{E_F}^{\infty}\frac{J_{W_S}(E')}{(E'-E_F)(E-E')}dE' , \tag{7}$$

$$J_{\Delta V_D}(E)=(E_F-E)\frac{\text{P}}{\pi}\int_{E_F}^{\infty}\frac{J_{W_D}(E')}{(E'-E_F)(E-E')}dE' , \tag{8}$$

where $J_{W_S}(E')$ and $J_{W_D}(E')$ ar the volume integrals per nucleon of the imaginary volume and surface potentials, respectively. Accordingly we rewrite Eq. (2) as

$$\begin{aligned} U_D(r,E)&=V(r,E)+iW(r,E)=V_0(r,E)+\Delta V_S(r,E)+\Delta V_D(r,E)+iW_S(r,E)+iW_D(r,E)\\ &=V_0(E)f(r,R_0,a_0)+\Delta V_S(E)f(r,R_S,a_S)-4a_D\Delta V_D(E)\frac{d}{dr}f(r,R_D,a_D)\\ &\quad +iW_S(E)f(r,R_S,a_S)-i4a_D W_D(E)\frac{d}{dr}f(r,R_D,a_D) , \end{aligned} \tag{9}$$

where $f(r,R_j,a_j)$ with $j=0,S,D$ represents the functional Woods-Saxon dependence. The volume integrals of the imaginary potential used in Eqs. (7) and (8) are obtained at a given energy from a best-fit analysis with the standard optical model. The geometry for $\Delta V_S(r,E)$ and $\Delta V_D(r,E)$ use the parameters of $W_S(r,E)$ and $W_D(r,E)$, respectively, and the potential depths $\Delta V_S(E)$ and $\Delta V_D(E)$ are given by

$$\Delta V_S(E)=\frac{J_{\Delta V_S}}{\int f(r,R_S,a_S)d\mathbf{r}}\ , \tag{10}$$

$$\Delta V_D(E)=\frac{J_{\Delta V_D}}{4a_D\int(d/dr)f(r,R_D,a_D)d\mathbf{r}}\ . \tag{11}$$

We apply the dispersion analysis just to the central part of the deuteron-nucleus potential, keeping the spin-orbit term $U_{\text{s.o.}}(r,E)$ unchanged from its form in the standard OMP. The Thomas form factor is used as

$$U_{\text{s.o.}}(r,E)=2V_{\text{s.o.}}\frac{1}{r}\frac{d}{dr}f_{\text{s.o.r.}}(r,R_{\text{s.o.r.}},a_{\text{s.o.r.}})\boldsymbol{l}\cdot\mathbf{s}$$
$$+i2W_{\text{s.o.}}\frac{1}{r}\frac{d}{dr}f_{\text{s.o.i.}}(r,R_{\text{s.o.i.}},a_{\text{s.o.i.}})\boldsymbol{l}\cdot\mathbf{s}\ . \tag{12}$$

In the present analysis, only the real term appears.

IV. INDIVIDUAL BEST FIT USING A DISPERSIVE OMP

In the re-analysis for the cross section and analyzing power data in the dispersive OMP frame, the volume integrals of the surface and volume imaginary potentials, $J_{W_D}(E)$ and $J_{W_S}(E)$, are fixed to the values given by the best-fit optical potentials reported in Refs. [11–16]. These values are plotted in the upper part of Fig. 2. The $J_W(E)$ values are a measure of the absorption for the incident flux, and it is expected that these values are more stable than the individual OMP geometrical parameter values. In the upper part of Fig. 2, the filled circles, vertical crosses, and diamonds refer to the J_W, J_{W_S}, and J_{W_D} terms, respectively. The horizontal axis (E) in Fig. 2 refers to the incident deuteron energy when $E>0$, and the binding energy between an n-p pair and the nucleus ^{208}Pb when $E<0$. At $E=E_F$ the absorptive potential of the n-p pair is expected to vanish [1]. This has been shown as one additional filled circle in this plot. Below $E=40$ MeV, the individual best-fit volume imaginary potential values are reported to be zero.

For the dispersive OMP analysis it is useful to represent the energy variations of the volume integrals J_{W_S} and J_{W_D} in suitable functional forms. Following the schematic model of Jeukenne and Mahaux [20], the energy dependence of the integrals for these best-fit imaginary volume and surface potentials $J_{W_S}(E)$ and $J_{W_D}(E)$ have each been described using the parametrizations [20]

$$J_{W_D}(E)=a\frac{(E-E_F)^4}{(E-E_F)^4+b^4}e^{-c(E-E_F)} \tag{13}$$

and

$$J_{W_S}(E)=d\frac{(E-E_F)^4}{(E-E_F)^4+e^4}\ . \tag{14}$$

In producing the curves in the top part of Fig. 2, we use the following parameter values: $a=135.0$ MeV fm^3, $b=25.56$ MeV, $c=0.01191$ MeV^{-1}, $d=76.21$ MeV fm^3, and $e=93.16$ MeV.

Equations (7), (8), (13), and (14) are the essential inputs for the dispersive OMP calculations. The bottom part of Fig. 2 contains the curves corresponding to $J_{\Delta V_S}$ and $J_{\Delta V_D}$ values as functions of energy between -16 and 100 MeV. The volume correction term $J_{\Delta V_S}$ is always positive at $E>0$, and the surface correction term $J_{\Delta V_D}$ crosses zero at $E=25$ or 12.5 MeV/nucleon. This behavior is similar to that seen for nucleon-nucleus scattering [5].

The values of the correction terms $J_{\Delta V_S}$ and $J_{\Delta V_D}$ were fixed during the search of the geometrical parameters for the dispersive best-fit OMP. This constrains the potential depths $\Delta V_S(E)$ and $\Delta V_D(E)$ to the values calculated from Eqs. (10) and (11). Similarly the imaginary potential depths $W_S(E)$ and $W_D(E)$ are calculated from

$$W_S(E)=\frac{J_{W_S}}{\int f(r,R_S,a_S)d\mathbf{r}} \tag{15}$$

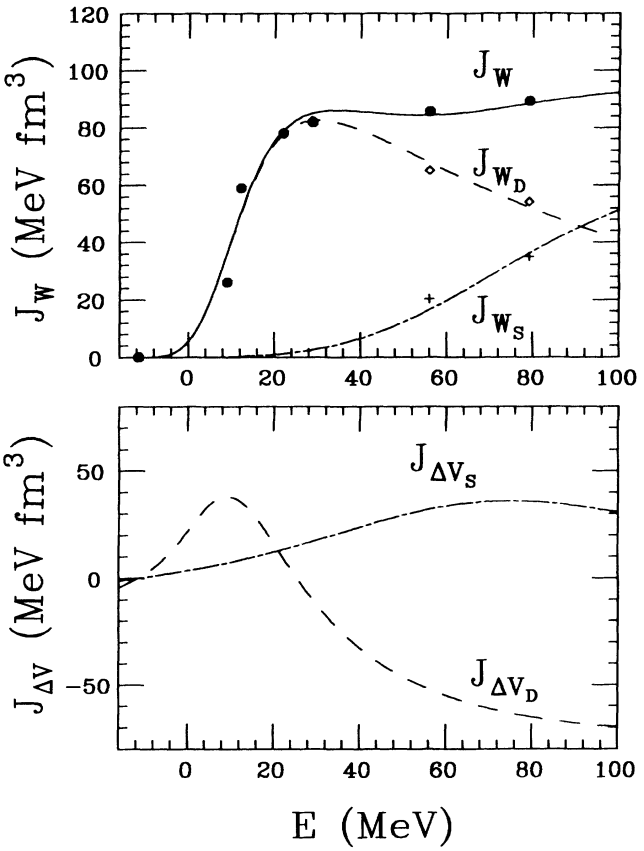

FIG. 2. In the upper plot, the filled-circle, cross, and diamond points represent the volume integrals of the imaginary potentials of $J_W(E)$, $J_{W_S}(E)$, and $J_{W_D}(E)$, respectively, from best-fit analyses. The analytic parametrizations of the energy dependence of $J_{W_D}(E)$ and $J_{W_S}(E)$ are shown by the dashed and dot-dashed curves, respectively. The energy dependence curves of the volume correction term $J_{\Delta V_S}(E)$ and the surface correction term, $J_{\Delta V_D}(E)$, calculated using the dispersion relation, are shown in the lower plot.

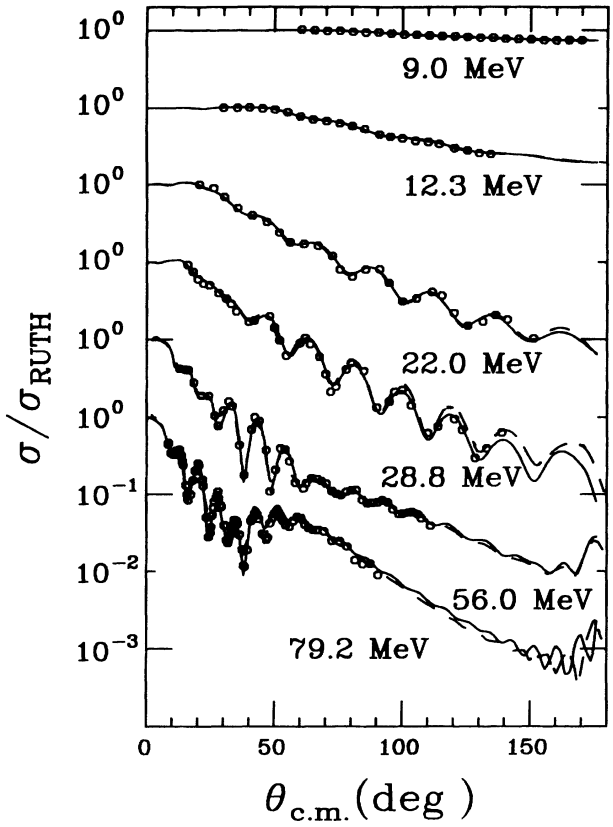

FIG. 3. Angular distributions of the cross section (ratio to Rutherford) for deuteron elastic scattering from ^{208}Pb. The circles indicate experimental data. The solid lines are the best-fit results using the dispersive OMP and the dashed lines are the best-fit standard optical potentials reported in Refs. [11–16].

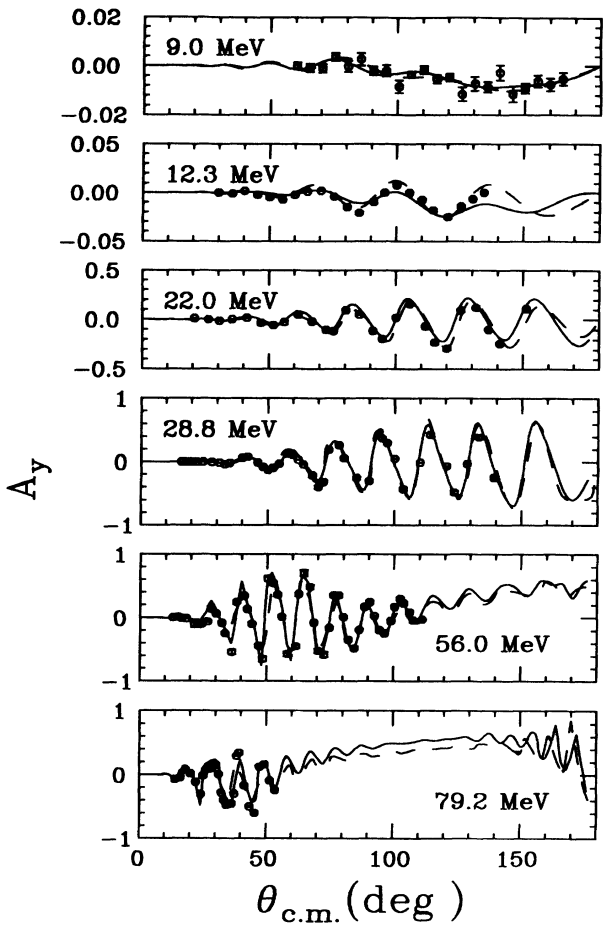

FIG. 4. As in Fig. 4, but for vector analyzing powers.

and

$$W_D(E)=\frac{J_{W_D}}{4a_D\int(d/dr)f(r,R_D,a_D)d\mathbf{r}} . \quad (16)$$

The other parameters, including the real central and spin-orbit depths as well as the radial shape of the imaginary potential, were allowed to vary. This gave ten adjustable parameters

$$(V_0,r_0,a_0,r_S,a_S,r_D,a_D,V_{\text{s.o.}},r_{\text{s.o.r.}},a_{\text{s.o.r.}}) ,$$

the same number as the standard OMP

$$(V,r_V,a_V,W_S,W_D,R_W,a_W,V_{\text{s.o.}},r_{\text{s.o.r.}},a_{\text{s.o.r.}})$$

TABLE I. Best-fit dispersive optical model parameters.

E (MeV)	9	12.3	22	28.8	56	79.2
V_0	99.84	95.99	88.47	85.15	81.55	76.29
r_0	1.217	1.194	1.217	1.221	1.223	1.221
a_0	0.458	0.409	0.661	0.805	0.873	1.015
W_S	0.05	0.08	0.31	0.61	3.69	5.56
ΔV_S	1.81	2.16	3.28	4.04	7.19	5.52
r_S	1.217	1.216	1.217	1.250	1.257	1.438
a_S	0.458	0.503	0.661	0.495	0.682	0.607
W_D	5.83	7.30	12.13	12.77	10.99	6.65
ΔV_D	6.18	5.17	1.60	−1.42	−8.39	−8.25
r_D	1.667	1.553	1.262	1.320	1.257	1.258
a_D	0.520	0.667	0.911	0.848	0.887	1.100
$V_{\text{s.o.}}$	8.11	3.27	5.71	5.38	6.31	5.39
$r_{\text{s.o.r.}}$	1.07	1.036	1.07	1.00	0.837	1.167
$a_{\text{s.o.r.}}$	0.66	0.45	0.66	0.40	1.00	0.55

[11–16]. Despite the similarity in the number of adjustable parameters, the dispersive optical model brings additional physical constraints to the description of the elastic scattering, resulting in a more self-consistent model.

In order to carry out the analysis, the computer code SNOOPY8Q [21] was modified [22] to include the form of the central part of the dispersive optical potential $U_D(r,E)$ as defined in Eq. (9). The individual best-fit parameters in this dispersive analysis were obtained when the minimum $\chi^2_{\rm tot}$ was achieved for the difference between the cross-section and analyzing power data and their calculated values.

The experimental values and relative uncertainties of the cross-section and analyzing power data at $E_d=9.0$ and 79.2 MeV are available [11,16] and were used in searches conducted at individual energies. The data sets at $E_d=12.3$, 22.0, 28.8, and 56.0 MeV were not available in numerical form and were read from the graphs in the publications cited. Although done with care, this method introduced additional uncertainties estimated at up to 5%. We assigned equal uncertainties (5% for $\theta \leq 50°$ and 10% for larger angles) to all data points at $E_d=12.3$, 22.0, 28.8, and 56.0 MeV. In this context, a comparison of χ^2 for different analyzing methods, such as dispersive and standard optical potentials, applied to this data set would be meaningful, but not a comparison of the χ^2 between data sets with different assigned uncertainties.

In our dispersive best-fit parameter search, initial values for $V_0, r_0, a_0, r_D, a_D, V_{\rm s.o.}, r_{\rm sor}$, and $a_{\rm sor}$ were set to the values given by potential L form the global analysis of Daehnick [17]. The initial parameters r_S and a_S were set to the same values as r_0 and a_0, respectively. The absorptive potential depths, W_S and W_D, were calculated using Eqs. (15) and (16). The best-fit dispersive OMP parameters are listed in Table I. The cross sections (ratio to Rutherford) and vector analyzing powers calculated using these parameters are shown in Figs. 3 and 4, respectively. The best-fit dispersive OMP provides fits of simi-

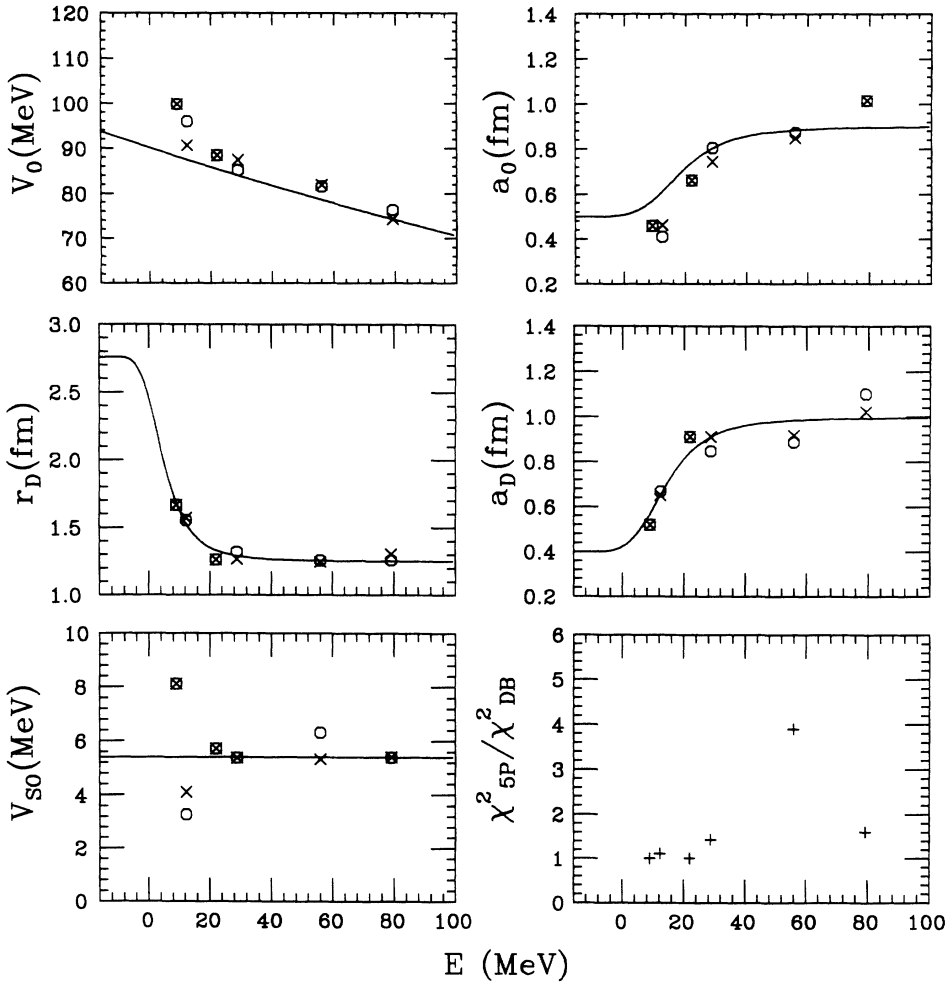

FIG. 5. The circles and diagonal crosses are geometrical parameters and potential depths of the dispersive OMP for $d+^{208}$Pb as determined from the best-fit and five-parameter searches, respectively. The solid lines represent parametrization of geometrical parameters and potential depths used in our dispersive OMP with smooth energy dependence as defined in Eq. (21). In the bottom right figure, the vertical crosses refer to the ratio of χ^2 for the five-parameter (5P) to best-fit (DB) dispersive calculations.

lar quality to those obtained with the standard parametrization [11–16] shown by the dashed lines in Figs. 3 and 4.

The best-fit dispersive OMP parameters V_0, a_0, r_D, a_D, and $V_{s.o.}$ are shown as circles in Fig. 5 (see Sec. V for other symbols in this figure). We make the following observations.

(i) The geometry of the real central potential $V_0(r,E)$. The variation of r_0 with E (not shown in Fig. 5) in the energy interval between 9 and 79.2 MeV is rather small, ranging from 1.194 to 1.223 fm. However, the parameter a_0 shows a strong energy dependence; its value increases more than twice in the same energy interval.

(ii) The geometry of the imaginary central potential. Significantly larger r_D radii, and smaller a_D diffusenesses, are needed to achieve best fits for the data sets $E=9.0$ ($r_D=1.667$, $a_D=0.52$ fm) and 12.3 MeV ($r_D=1.553$, $a_D=0.667$ fm) compared to the higher energies. This trend of r_D is consistent with the geometrical parameters r_D obtained in a standard OMP best-fit analysis [11–16]. No smooth energy dependence is observed for the rest of the geometrical parameters of the central potential, such as r_S and a_S.

(iii) The potential depth $V_0(E)$. Values of $V_0(E)$ increase as the energy decreases in a smooth, nearly linear way.

(iv) The spin-orbit term $V_{s.o.}(r,E)$. No smooth energy dependence is observed for the geometrical parameters $r_{s.o.r.}$ and $a_{s.o.r.}$ as well as the potential depth $V_{s.o.}$. This is consistent with the results obtained in the best fit using a standard OMP [11–16].

In order to get a better understanding of this dispersive OMP, it is useful to compare the dispersive and standard OMP's in terms of the radial shapes of the real central potential $V(r,E)$, its volume integrals, and root-mean-square (rms) radii. The following are our observations.

(i) Radial shapes of the real central potential. The real potential radial shapes are shown in Fig. 6. The solid lines at each energy are the total potential, which is the sum of the terms (shown as dashed lines) from the central, "Hartree-Fock" piece $V_0(1)$, the surface correction $\Delta V_D(2)$, and the volume correction $\Delta V_S(3)$. The dot-

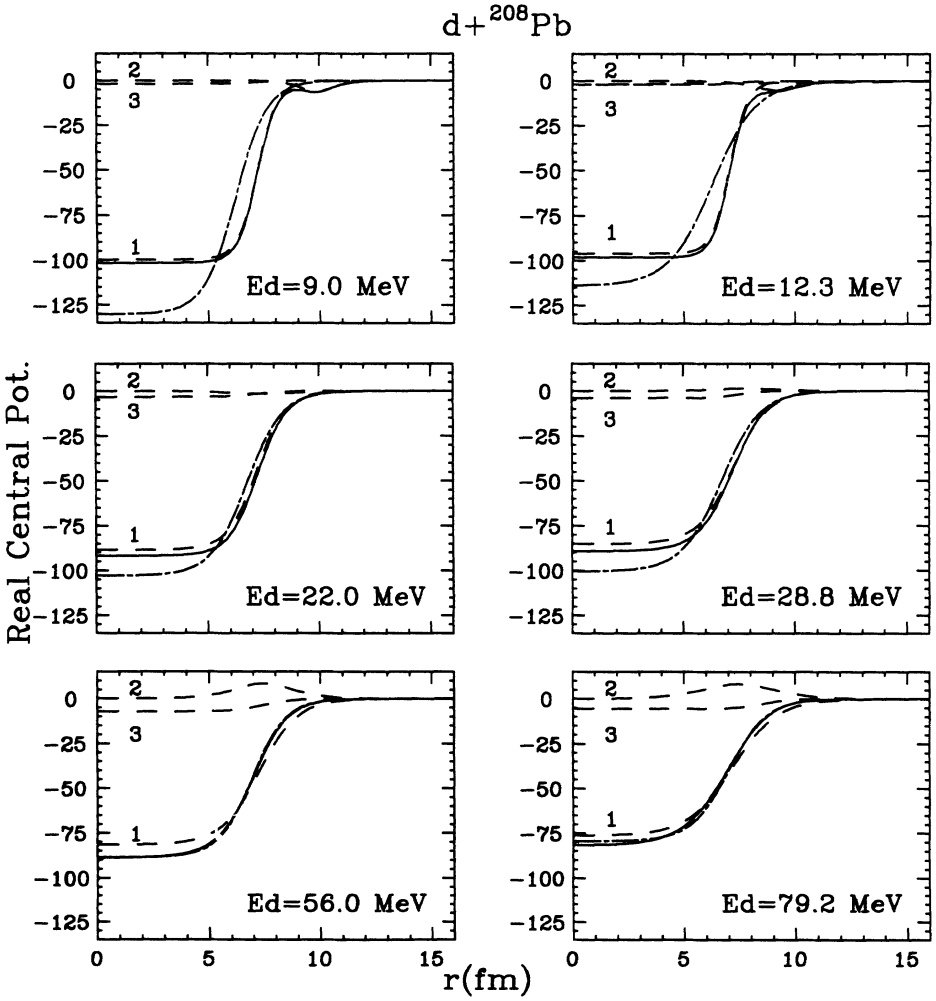

FIG. 6. Radial dependence of the real central optical potential terms. The dashed curves marked 1, 2, and 3 refer to the $V_0(r)$ (central), $\Delta V_D(r)$ (surface correction), and $\Delta V_V(r)$ (volume correction) contributions, respectively. The solid and dot-dashed lines are the full real central potentials in the dispersive and standard optical models, respectively.

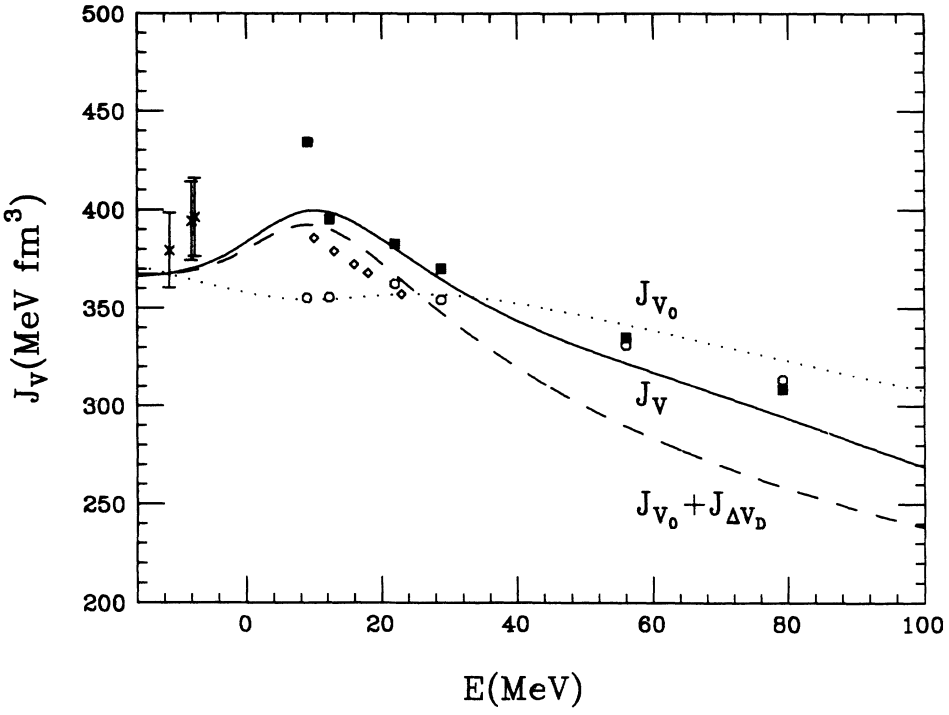

FIG. 7. Energy dependence of the volume integrals of the real central potential. The open circles and filled squares are given by the best fits of the standard and dispersive OMP, respectively. The solid curve is given by the full potential $J_V = J_{V_0} + J_{\Delta V_S} + J_{\Delta V_D}$. The dotted line refers to the term $J_{V_0}(E)$. The dashed line represents the sum of the two terms $J_{V_0}(E)$ and $J_{\Delta V_D}(E)$. The diamonds refer to the optical potential set III described in Sec. II, and the diagonal crosses are the sum of the volume integrals of the proton and neutron bound states, which are located in bound-state orbits corresponding to correlated, two-particle state configurations observed in (α,d) and (d,α) reactions [24–25], with a scaling factor 0.85.

dashed line is the standard best-fit optical potential used to obtain the original volume integrals. At lower incident deuteron energies, the best-fit real central dispersive potentials are shallower and extend to larger radii than those obtained from the standard OMP. Here, the interaction between the incident deuteron and the nucleus is located primarily in the surface region of the nucleus. This is progressively reflected in the energy dependence of the shape of the dispersive part of the central potential. The dispersive part of the central potential at $E_d = 9.0$ and 12.3 MeV has a small dip (at $r = 10$ fm) in the surface region. While this may appear to be a nonphysical shape, it is also likely that the deuteron is largely insensitive to its details. At 9.0 MeV, a semiclassical calculation indicates that the deuteron does not approach any closer than 12.9 fm to the nucleus because of the repulsive character of the Coulomb and centrifugal barriers. The situation at 12.3 MeV may not be greatly different. Only the lowest partial waves ($L \leq 6$) have sufficient bombarding energy to penetrate the nuclear interior, and in a standard optical-model analysis these partial waves are strongly absorbed. Thus, these potential shapes may serve only two purposes. The first is to provide sufficient attraction at large distances to account for the values of the cross sections in Fig. 3 that are smaller than the Rutherford cross section. Second, they provide a volume integral of the size required to obtain the proper phase shifts in each partial wave. If the two criteria are met, details of the radial shape inside the Coulomb turning point radius may not be important.

(ii) The volume integrals of the real central potential. It is important to study the properties of the volume integrals of the potentials, which incorporate the energy dependence of the geometry as well as the potential depths of the dispersive OMP. The volume integral of the full real central potential per nucleon, $J_V(E)$, resulting from the dispersive (filled squares) and standard (open circles) parametrizations are shown in Fig. 7. The deviations of the real volume integral of the dispersive OMP from that of the standard OMP become larger at lower deuteron energies. Also shown are smooth parametrizations of the terms in the real central optical potential. The integral J_{V_0} (dotted line) follows closely the standard OMP values. The solid curve results from the addition of surface and volume corrections to J_{V_0} and follows the dispersive volume integrals. In the dashed line, the sum of J_{V_0} and the surface correction $J_{\Delta V_D}$ is represented. Most of the deviation from the standard OMP is seen to result from the surface correction term in the dispersive OMP. This absorption occurs at a large radius for the smaller incident deuteron energies, and is responsible for the appearance of the extra attractive surface dip in Fig. 6.

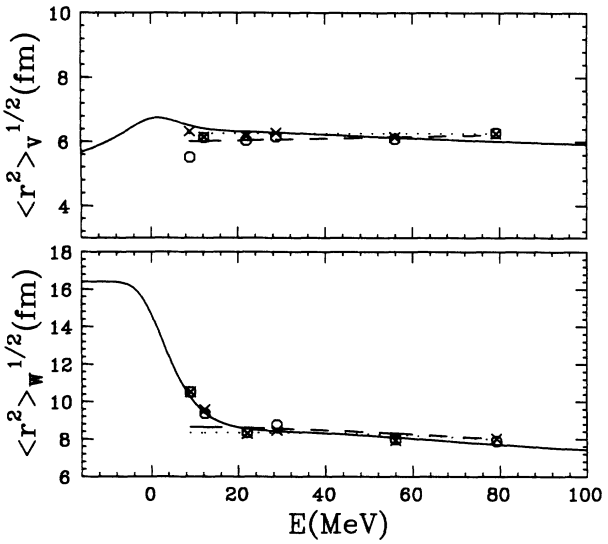

FIG. 8. Energy dependences of the real, V, and imaginary, W, rms radii. The open circles and diagonal crosses represent the best-fit values of the standard and dispersive OMP, respectively. The solid lines refer to the calculation given by the dispersive OMP defined in Eq. (2). The dashed and dotted lines are given by the deuteron global OMP reported in Refs. [17] and [19], respectively.

(iii) The rms radii of the central potential. The energy dependence of the rms radii obtained in the best fit of the dispersive and standard OMP are shown as open circles and diagonal crosses in Fig. 8, respectively. The rms radii have similar energy dependences in both models. At energies below 16 MeV, $\langle r^2 \rangle_W$ from global potentials fall well below the best-fit results.

V. $d+^{208}$Pb DISPERSIVE OMP WITH SMOOTH ENERGY DEPENDENCE

In this section, the development of a dispersive OMP with a smooth energy dependence for all the parameters is explored. This is necessary to reliably extrapolate to the negative-energy region and to obtain OMP parameters at any positive energy below 90 MeV. In this model, the geometrical parameters in the real volume correction term are kept at the same values as that of the real potential $V_0(r,E)$, i.e., $r_S=r_0$ and $a_S=a_0$. This is the same prescription used in the nucleon-nucleus dispersive OMP analysis [5]. No energy dependence of the real radius r_0 is assumed, and its initial value is the average value (1.216 fm) of r_0 at the six energies listed in Table I. Because no smooth energy dependence for the spin-orbit geometrical parameters was obtained, neither in the best-fit standard nor in the dispersive OMP, the values $r_{\text{s.o.r.}}$ and $a_{\text{s.o.r.}}$ were fixed at $r_{\text{s.o.r.}}=1.07$ fm and $a_{\text{s.o.r.}}=0.66$ fm, the same values used in Daehnick's global OMP [17].

A five-parameter (V_0, a_0, r_D, a_D, and $V_{\text{s.o.}}$) search was performed for each energy data set. The potential depths W_S, W_D, ΔV_S, and ΔV_D were determined using the same method as described in Sec. III for the dispersive OMP best fits. A grid search was conducted on the real radius r_0 with step size 0.001. For each value of r_0 (from 1.206 to 1.226), the five-parameter search was performed for each energy data set. A best value of $r_0=1.221$ fm was chosen. We present in Fig. 5 values obtained for the five dispersive OMP parameters (diagonal crosses) as a function for the deuteron energy. The results of the five-parameter search show that V_0, a_0, r_D, and a_D have strong energy dependences. The real spin-orbit potential depth $V_{\text{s.o.}}$ shows no strong energy dependence, and its average value is $V_{\text{s.o.}}=5.7$ MeV. Taking guidance from the dispersive OMP parameters obtained in the best fit and the results of the five-parameter search, the mathematical forms of the parametrization equations for $V_0(E)$, $a_0(E)$, r_{W_D}, and a_{W_D} were chosen.

The $V_0(E)$ potential depth was assumed to have the form

$$V_0(E)=V_0(E_F)\exp\left[\frac{\alpha(E-E_F)}{V_0(E_F)}\right]. \tag{17}$$

For $a_0(E)$, $r_D(E)$, and $a_D(E)$, the functional form was

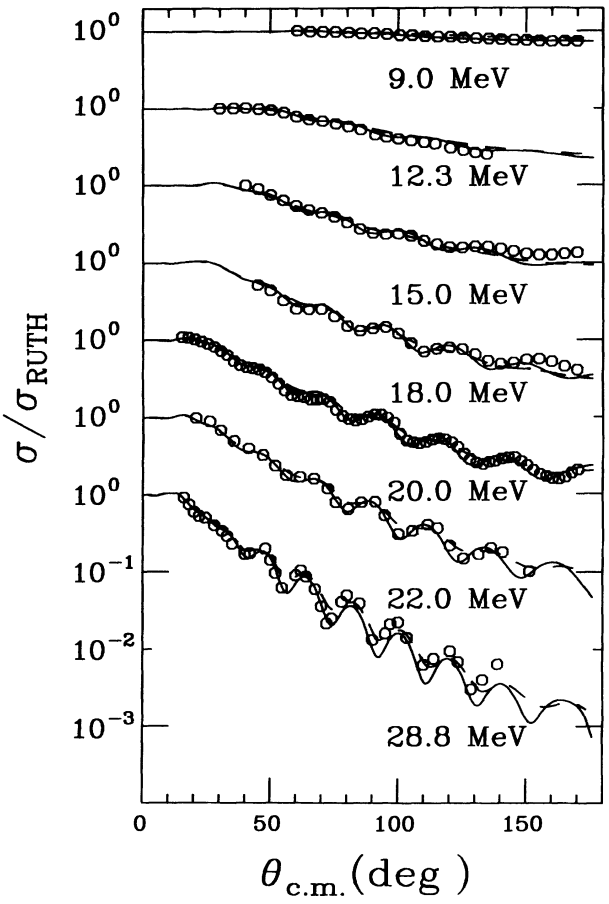

FIG. 9. Comparisons between the $d+^{208}$Pb experimental cross section (ratio to Rutherford) and the calculation based on the dispersive OMP defined in Eq. (21) for $E_d<30$ MeV. The calculations given by the deuteron global model reported in Ref. [17] are plotted in this figure as dashed curves.

taken to be

$$a_0(E)=a_0(E_F)+\frac{b(E-E_F)^4}{(E-E_F)^4+c^4}\ , \tag{18}$$

$$r_D(E)=r_D(E_F)-\frac{d(E-E_F)^4}{(E-E_F)^4+e^4}\ , \tag{19}$$

and

$$a_D(E)=a_D(E_F)+\frac{f(E-E_F)^4}{(E-E_F)^4+g^4}\ . \tag{20}$$

Values of the parameters $V_0(E_F)$, α, $a_0(E_F)$, b, c, $r_D(E_F)$, d, e, $a_D(E_F)$, f, and g were chosen to follow the energy dependence shown in Fig. 5. Several of the parameter values fell away from these smooth curves. Realizing that such deviations might be the result of correlations among the parameters, additional grid searches were made in which one parameter was allowed to vary while the others were fixed at the values given by the functional form. The parameters V_0, a_0, r_D, a_D, and $V_{s.o.}$ were varied in this way. In many cases, values closer to the smooth curve resulted. This procedure was repeated resulting in the curves of Fig. 5 and the OMP values shown by the crosses. The variation of a_0 with energy was reduced since values less than 0.4 fm did not appear to be physically reasonable, and the calculations below 20 MeV appeared to be less sensitive to the choice of a_0 than the calculations at higher energies (except the calculation at 79 MeV). The resulting dispersive OMP for $d+^{208}$Pb with a smooth energy dependence can be written as

$$V_0(E)=92.73\exp\left[\frac{-0.227(E-E_F)}{92.73}\right]\ \text{MeV}\ ,$$

$$r_0=1.221\ \text{fm}\ ,$$

$$a_0(E)=0.5+\frac{0.4(E-E_F)^4}{(E-E_F)^4+30.3^4}\ \text{fm}\ ,$$

$$r_D(E)=2.76-\frac{1.51(E-E_F)^4}{(E-E_F)^4+16.39^4}\ \text{fm}\ , \tag{21}$$

$$a_D(E)=0.4+\frac{0.597(E-E_F)^4}{(E-E_F)^4+25.87^4}\ \text{fm}\ ,$$

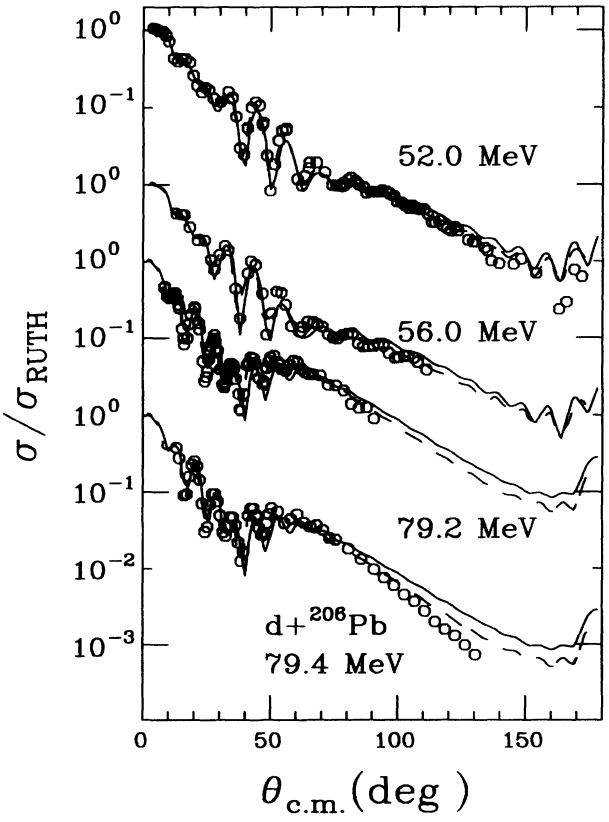

FIG. 10. As in Fig. 9, but for E_d at higher energies. The bottom set of data is from $d+^{206}$ Pb.

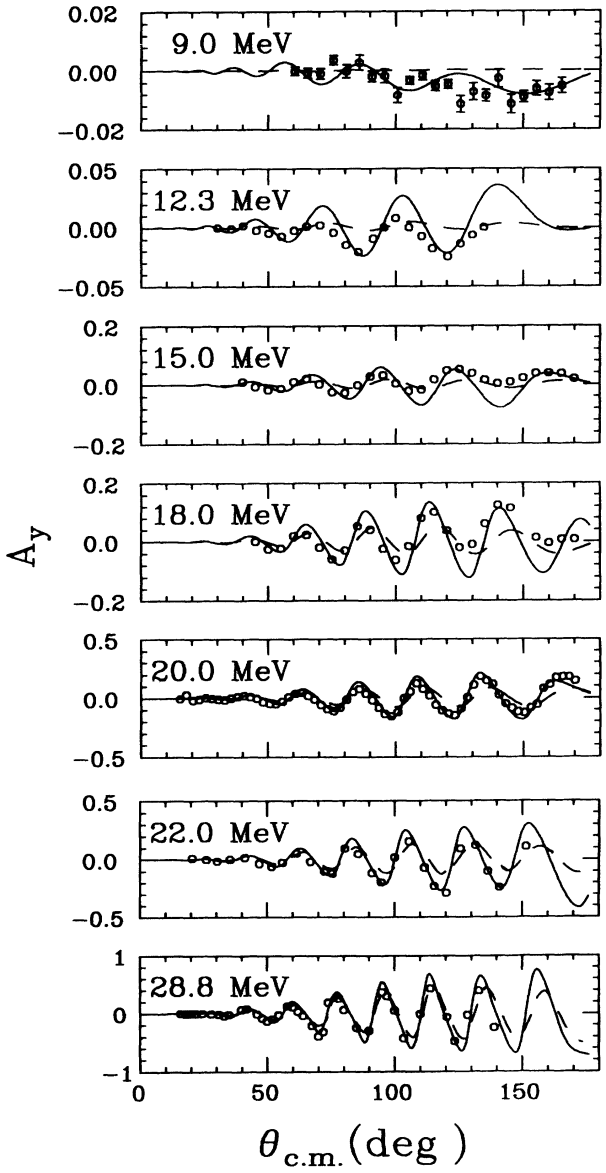

FIG. 11. As in Fig. 9, but for vector analyzing powers.

$$J_{W_D}(E)A_d = 271.89\frac{(E-E_F)^4}{(E-E_F)^4+25.56^4} \times e^{-0.01191(E-E_F)}\ \text{MeV fm}^3\ ,$$

$$J_{W_S}(E)A_d = 153.49\frac{(E-E_F)^4}{(E-E_F)^4+93.16^4}\ \text{MeV fm}^3\ ,$$

and $V_{\text{s.o.}}=5.4$ MeV, $r_{\text{s.o.}}=1.07$ fm, and $a_{\text{s.o.}}=0.66$ fm. In Eq. (21), A_d is the deuteron mass.

We expect this potential to give a reasonably good description of the experimental data at energies $E<90$ MeV. It may be extrapolated to the negative-energy region. At this point, it is not clear how to proceed to the study of bound n-p pair properties using our potential. Some comments on this subject are provided in the next section.

Comparisons between the experimental deuteron elastic data (circles) containing both cross sections (ratio to Rutherford) and analyzing power data at $9\le E_d\le 80$ MeV and the dispersive OMP predictions (solid curves) as described in Eq. (21) are presented in Figs. 9–12. The calculations based on Daehnick's deuteron global OMP are also presented as dashed curves. The dispersive OMP gives a good description of the experimental data. The data sets at $E_d=15$ and 18 MeV were extracted from the graphs in Ref. [10]. The data sets at $E_d=20$ and 52 MeV are given by Grabmayr [18] in numerical form. In the bottom parts of Figs. 10 and 12, the circles are the experimental data for $d+^{206}$Pb. In this data set [23], the cross sections and vector analyzing power measurements have been extended to larger angles than in the $d+^{208}$Pb data set at the same energy. The same dispersive OMP parameters are used in the calculations for $d+^{208}$Pb at $E_d=79.2$ MeV and $d+^{206}$Pb at $E_d=79.4$ MeV. A better description to the cross-section and analyzing power data at large angle for 79 MeV may be achieved [16,23] if an additional imaginary spin-orbit potential is used.

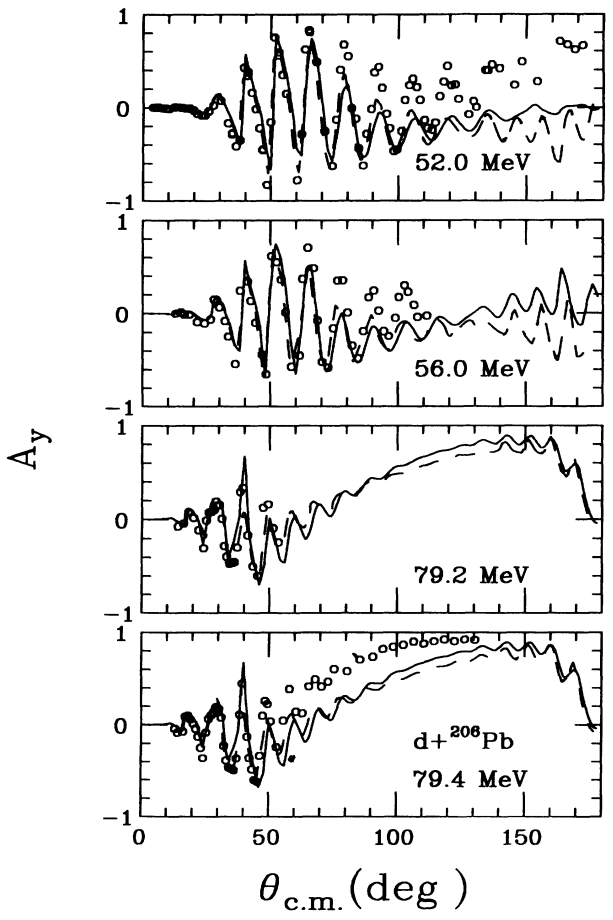

FIG. 12. As in Fig. 10, but for vector analyzing powers.

VI. DISCUSSION

In this section we present a discussion of the properties of the dispersive OMP given by Eq. (21) in terms of volume integral, rms values, and reaction cross sections. The open circles and filled squares in Fig. 7 represent the best-fit standard and dispersive OMP values, respectively. The diamonds refer to the data reported by Murayama *et al.* [10]. The sold line is the real volume integral of the full real central potential $J_V(E)$ given by the dispersive OMP with a smooth energy dependence [Eq.(21)]. The dotted line is the $J_{V_0}(E)$ term and the dashed line refers to the sum of the $J_{V_0}(E)$ and $J_{\Delta V_D}(E)$ terms.

Also in Fig. 7, the diagonal crosses in the negative-energy region are the estimated real volume integrals for the n-p pairs as a function of the binding energies of the n-p pairs in the nucleus. The n-p pairs are located in bound-state orbits corresponding to correlated two-particle state configurations observed in the (α,d) and (d,α) reactions [24,25] on ^{208}Pb. The three two-particle states (dominant configurations) are the $(\pi 2f_{7/2},\nu 2g_{9/2})$ and $(\pi 1i_{13/2},\nu 2g_{9/2})$ observed in the ^{208}Pb$(\alpha,d)^{210}$Bi reaction [24] at $E_x=0.915$ and 1.316 MeV, and the $(\pi 3s_{1/2},\nu 3p_{1/2})$ in the ^{208}Pb$(d,\alpha)^{206}$Ti reaction [25] at $E_x=0.304$ MeV. The binding energies of the observed n-p pair states in the ^{210}Bi nucleus are evaluated by

$$E_b=-Q[^{210}\text{Bi}(\gamma,pn)]+E_x[^{208}\text{Pb}(\alpha,d)^{210}\text{Bi}]\ , \quad (22)$$

and in the ^{208}Pb nucleus by

$$E_b=-Q[^{208}\text{Pb}(\gamma,pn)]+E_x[^{208}\text{Pb}(d,\alpha)^{206}\text{Ti}]\ , \quad (23)$$

where the experimental Q values in Ref. [26] are used. The estimated volume integrals of the real potential for the n-p pairs are the sum of the volume integrals [5,6] of the n and p, which are located in the bound-state orbits specified in the two-particle state configurations. These values have been scaled down by 15±5% as suggested in Ref. [27], where the comparison between the deuteron optical potential and the sum of neutron and proton potentials was made in the positive-energy region. The dispersive OMP defined in Eq. (21) (solid line) gives a reasonable fit for the deuteron elastic scattering as well as the n-p pair bound states in terms of the volume integral for the central potential.

The rms radii of the real and imaginary central poten-

tials are given as

$$\langle r^2\rangle_V^{1/2} = \left[\frac{J_{V_0}\langle r^2\rangle_{V_0}+J_{\Delta V_S}\langle r^2\rangle_{\Delta V_S}+J_{\Delta V_D}\langle r^2\rangle_{\Delta V_D}}{J_V}\right]^{1/2} \quad (24)$$

and

$$\langle r^2\rangle_W^{1/2} = \left[\frac{J_{W_S}\langle r^2\rangle_{W_S}+J_{W_D}\langle r^2\rangle_{W_D}}{J_W}\right]^{1/2}, \quad (25)$$

where J_V is the sum of the three terms J_{V_0}, $J_{\Delta V_S}$, and $J_{\Delta V_D}$, and J_W is the sum of the two terms J_{W_S} and J_{W_D}. The values of the $\langle r^2\rangle_V^{1/2}$ and $\langle r^2\rangle_W^{1/2}$, as functions of the energy E and calculated using the dispersive OMP defined in Eq. (21), are plotted in Fig. 8. The predictions given by the global deuteron OMP from Refs. [17,19] are also shown.

Two comprehensive deuteron reaction cross-section studies using attenuation techniques were performed at 22.4 MeV by Wilkens and Igo [28] and at 26.5 MeV by Mayo *et al.* [29]. The experimental deuteron reaction cross sections for ^{208}Pb at these two energies are plotted in Fig. 13. The prediction of the reaction cross section using the dispersive OMP defined in Eq. (21) is shown in Fig. 13 as a solid curve. The dashed and dotted curves are the predictions given by the Daehnick [17] (set L) and Bojowald [19] global model parameters. The three curves have similar shapes. All models overpredict the 26.5-MeV σ_R data by about 20% and the 22.4-MeV σ_R data by about 30%. In this analysis, we did not use the experimental reaction cross sections as part of the data to obtain the potential parameters because of the unsuccessful attempts to predict these values for σ_R reported in Ref. [17].

VII. SUMMARY

In the present work, a set of dispersive OMP parameters are obtained by fitting the experimental cross section and analyzing power data at several energies. The dispersion relation is used to fix the volume integral of corrections to the real central potential based on the volume integral of the imaginary terms. A new "self-consistent" computational technique, which may be useful in the dispersion analysis of nucleon or heavy-ion scattering from nuclei, was used. With the same number of free parameters, the best-fit dispersive OMP parameters give similar quality fits to those obtained with the standard best-fit OMP parameters.

The energy-dependent analytic forms in the dispersive OMP give a good agreement with the empirical volume integrals, including estimates for three n-p bound levels. The volume integrals of the imaginary dispersive potentials fall well below those of the standard global poten-

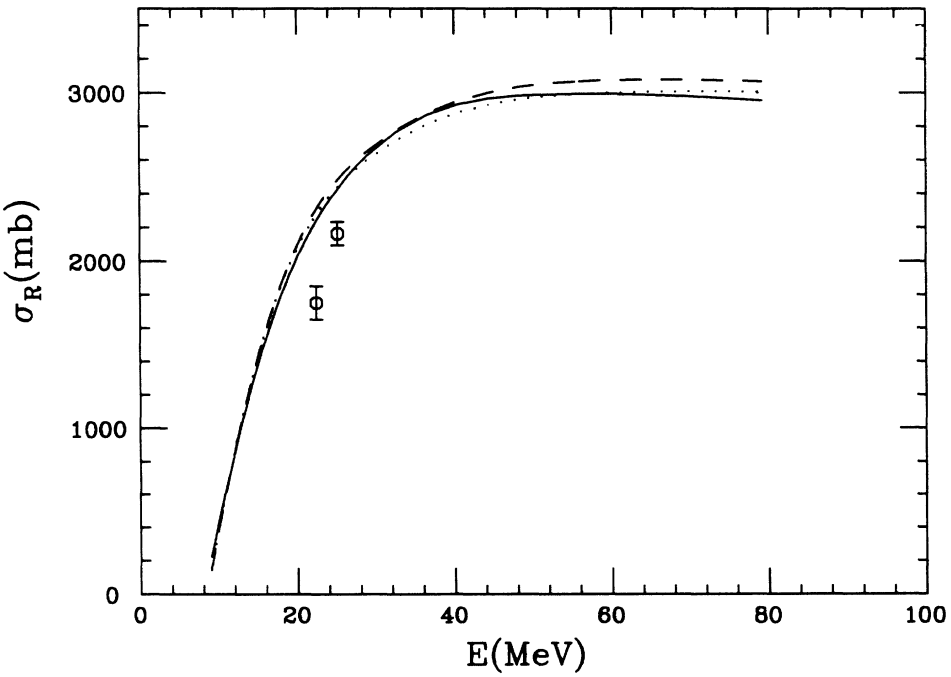

FIG. 13. The deuteron reaction cross sections σ_R on ^{208}Pb. The two data points are experimental reaction cross sections at deuteron energies E_d=22.4 and 26.5 MeV. The calculations for deuteron reaction cross sections on ^{208}Pb are shown as a solid curve [dispersive OMP defined in Eq. (21)], a dashed curve (OMP in Ref. [17]), and a dotted curve (OMP in Ref. [19]).

tials at energies below about 30 MeV. This energy dependence is consistent with the condition that the volume integrals of the imaginary potential must go smoothly to zero as the energy goes to the Fermi energy from above. This implies that the use of standard global potential model parameters at low energies may lead to significant errors.

ACKNOWLEDGMENTS

We are grateful to Dr. C. Mahaux for his comments. We owe special thanks to Dr. P. Grabmayr for providing the 20- and 52-MeV data sets. We also thank Dr. H. Nann and Dr. P. Schwandt, for their useful suggestions and comments.

[1] C. Mahaux, H. Ngô, and G. R. Satchler, Nucl. Phys. **A449**, 354 (1986).
[2] C. Mahaux and H. Ngô, Nucl. Phys. **A378**, 205 (1982).
[3] J. P. Delaroche, Y. Wang, and J. Rapaport, Phys. Rev. C **39**, 391 (1989).
[4] C. Mahaux and R. Sartor, Nucl. Phys. **A503**, 525 (1989).
[5] C. H. Johnson, D. J. Horen, and C. Mahaux, Phys. Rev. C **36**, 2252 (1987).
[6] C. Mahaux and R. Sartor, Nucl. Phys. **A481**, 381 (1988).
[7] A. A. Ioannides and R. C. Johnson, Phys. Rev. C **17**, 1331 (1978).
[8] Y. Wang and J. Rapaport, Nucl. Phys. **A454**, 359 (1986).
[9] C. M. Perey and F. G. Perey, At. Data Nucl. Data Tables **17**, 1 (1976), and references therein.
[10] T. Murayama, Y. Tagishi, T. Sakai, M. Tomizawa, H. Nishikawa, and S. Seki, Nucl. Phys. **A486**, 261 (1988).
[11] L. D. Knutson and W. Haeberli, Phys. Rev. C **12**, 1469 (1975).
[12] S. E. Vigdor, R. D. Rathmell, H. S. Liers, and W. Haeberli, Nucl. Phys. **A210**, 70 (1973).
[13] R. Frick, H. Clement, G. Graw, P. Schiemenz, N. Seichert, and Sun Tsu-Hsun, Z. Phys. A **319**, 133 (1984).
[14] G. Perrin, Nguyen Van Sen, J. Arvieux, R. Darves-Blanc, J. L. Durand, A. Fiore, J. C. Gondrand, F. Merchez, and C. Perrin, Nucle. Phys. **A282**, 221 (1977).
[15] N. Matsuoka, H. Sakai, T. Saito, K. Hosono, M. Kondo, H. Ito, K. Hatanaka, T. Ichihara, A. Okihana, K. Imai, and K. Nisimura, Nucl. Phys. **A455**, 413 (1986).
[16] C. C. Foster, J. C. Collins, V. R. Cupps, D. L. Friesel, H. Nann, W. W. Jacobs, W. P. Jones, S. Kailas, M. Kaitchuck, P. Schwandt, E. J. Stephenson, and W. W. Daehnick, Indiana University Cyclotron Facility Scientific and Technical Report, 1985, p. 61.
[17] W. W. Daehnick, J. D. Childs, and Z. Vrcelj, Phys. Rev. C **21**, 2253 (1980), and references therein.
[18] P. Grabmayr, private communication.
[19] J. Bojowald, H. Machner, H. Nann, W. Oelert, M. Rogge, and P. Turek, Phys. Rev. C **38**, 1153 (1988), and references therein.
[20] J. P. Jeukenne and C. Mahaux, Nucl. Phys. **A394**, 445 (1983).
[21] P. Schwandt, computer code SNOOPY8Q, Indiana University Cyclotron Facility Internal Report No. 85-9, 1987.
[22] Y. Wang, computer code SNPQDR 1989, Indiana University Cyclotron Facility Internal Report No. 89-10 (in preparation).
[23] M. C. Radhakrishna, N. G. Puttaswamy, H. Nann, J. D. Brown, W. W. Jacobs, W. P. Jones, D. W. Miller, P. P. Singh, and E. J. Stephenson, Phys. Rev. C **37**, 66 (1988).
[24] W. W. Daehnick, M. J. Spisak, and J. R. Comfort, Phys. Rev. C **22**, 1906 (1981).
[25] W. W. Daehnick, M. J. Spisak, R. M. Delvecchio, and W. Oelert, Phys. Rev. C **15**, 594 (1977).
[26] A. H. Wapstra and G. Audi, Nucl. Phys. **A432**, 1 (1985).
[27] K. Hatanaka, K. Imai, S. Kobayashi, T. Matsusue, M. Nakamura, K. Nisimura, T. Noro, H. Sakamoto, H. Shimizu, and J. Shirai, Nucl. Phys. **A340**, 93 (1980).
[28] B. Wilkens and G. Igo, Phys. Lett. **3**, 48 (1962).
[29] S. Mayo, W. Schimmerling, M. J. Sametband, and R. M. Eisberg, Nucl. Phys. **62**, 393 (1965).